RSC Advances

PAPER

View Article Online
View Journal | View Issue

Cite this: *RSC Adv.*, 2017, **7**, 7973

Fabrication of curcumin-loaded mesoporous silica incorporated polyvinyl pyrrolidone nanofibers for rapid hemostasis and antibacterial treatment

Dejian Li,†[a] Wei Nie,†[b] Liang Chen,[b] Yingke Miao,[b] Xu Zhang,[a] Fancheng Chen,[a] Bin Yu,[a] Rongguang Ao,[a] Baoqing Yu*[a] and Chuanglong He*[b]

Nanofiber mats have been widely applied in various biomedical fields such as drug delivery, tissue repair and wound dressing. In this study, the curcumin-loaded mesoporous silica incorporated nanofiber mats were prepared using blend electrospinning of curcumin-loaded mesoporous silica nanoparticles (CCM-MSNs) and polyvinyl pyrrolidone (PVP) for hemostasis. The prepared mats were then evaluated to determine their structure, biocompatibility and antibacterial activity, especially focusing on the hemostatic effect using an *in vivo* liver injury model. The results showed that CCM-MSN loading ratios less than 8 wt% could be homogeneously dispersed in the PVP electrospun nanofibers. The *in vitro* studies demonstrated that the hybrid nanofiber mats had no obvious toxic effect on the growth of L929 cells. The hybrid nanofiber mats also exhibited enhanced *in vitro* antibacterial effects against methicillin-resistant *Staphylococcus aureus* (MRSA). The antibacterial effect of the hybrid nanofiber mats was further confirmed by *in vivo* experiments. Moreover, the *in vivo* hemostasis studies revealed that the hybrid nanofiber mats could rapidly transform into hydrogel when they contact with blood, and then activate the clotting system to stop the wound bleeding. Therefore, the CCM-MSN incorporated PVP nanofiber mats provide a practical possibility for nanofiber-based hemostatic materials with good biocompatibility and high antibacterial activity.

Received 25th November 2016
Accepted 16th January 2017

DOI: 10.1039/c6ra27319j

www.rsc.org/advances

1. Introduction

Hemorrhage of parenchymal organs is the leading cause of morbidity and mortality on the battle field or in other contexts of trauma.[1] In general, mechanical compression of the lesion is the most direct solution for hemostasis due to its decreased perfusion and clotting promotion. Alternatively, high temperature burning is commonly used in surgical hemostasis. However, these hemostasis methods have some defects that greatly limit their wide application. The hemostasis time of the mechanical compression is relatively long while heat-based hemostasis is destructive to tissue architecture and may induce potential inflammation in the wound site. Hence, several hemostasis materials including sponges and porous powders have been developed and widely used for hemostasis.[2] Nevertheless, many spongy materials including collagen, fibrinogen and thrombin are usually derived from animal and human origin, which may exert risk of viral infection.[3] On the other hand, although porous powders have large specific surface area to absorb blood platelets and activate the clotting system, most of them consist of minerals and would produce heat when encountering blood, thus leading to secondary injury at the wound.[2,4] Therefore, there is still a great challenge for developing new hemostatic agents with high stanching efficacy and low adverse tissue damage.[4]

Owing to their high levels of porosity, gas permeation, and surface-to-volume ratio, electrospun nanofibers have attracted extensive interests in tissue regeneration and drug delivery.[5] Several recent reports suggested that the well-developed nanofiber mats could promote the blood coagulation, making it favorable for hemorrhage control. For example, Huang *et al.*[6] found that the *in situ n*-octyl-2-cyanoacrylate (OCA) electrospun nanofibers provided a quick hemostasis on pig lung resection model. Moreover, Han *et al.*[7] also developed a multiple drug carrying bilayer electrospun nanofiber mats for intestinal vascular hemostasis. Up to now, it is accepted that the hemostatic effect of the electrospun nanofiber mats is mainly attributed to their high porosity and specific surface area.[8]

Although electrospun nanofiber mats are promising hemostatic materials for various trauma, its high specific surface area also increase probability of pathogen contamination.[9,10] Hence,

[a]*Department of Orthopedics, Shanghai Pudong Hospital, Fudan University Pudong Medical Center, 2800 Gongwei Road, Huinan Town, Pudong New Area, Shanghai 201301, China. E-mail: doctorybq@163.com; Fax: +86 021 6803 5001; Tel: +86 021 6803 5001*

[b]*College of Chemistry, Chemical Engineering and Biotechnology, Donghua University, 2999 North Renmin Road, Shanghai 201620, China. E-mail: hcl@dhu.edu.cn; Fax: +86 021 6779 2742; Tel: +86 021 6779 2742*

† Contributed equally.

it is desirable to improve the antibacterial activity of the nanofiber mats to extend their clinical applications. Since that more and more pathogens become drug-resistant strain induced by abuse of traditional antibiotics,[11] it also necessary to develop new agents with broad spectrum antibacterial activity for preventing infection when applying nanofiber mats on the bleeding lesion. In addition, the definite size of the nanofiber mats made them difficult to conform to the wound with deep, narrow and irregular shapes, which restricts the practical application of nanofiber hemostatic materials. Thus, it is important to develop ideal hemostatic materials for clinical application.

Polyvinylpyrrolidone (PVP) is a water-soluble and physiologically acceptable polymer which can be rapidly transformed into hydrogel.[12] Thus, PVP nanofiber mats are expected to conform to the wound with deep, narrow and irregular shapes. In recent years, mesoporous silica nanoparticle (MSN) has been proposed as an effective drug carrier due to its large pore volumes, high drug loading capacity and favorable biocompatibility.[13–15] Therefore, in order to combine the advantages of these two classes of materials, this paper developed an organic–inorganic hybrid hemostatic material by incorporating the curcumin-loaded mesoporous silica nanoparticles (CCM-MSNs) into PVP nanofiber mats using electrospinning. The resulting nanofiber mats were well-characterized by various techniques to confirm the biocompatibility and interactions between PVP and CCM-MSNs. The hemostatic efficacy of the hybrid nanofiber mats was further evaluated by *in vitro* and *in vivo* experiments, and their antibacterial and anti-inflammatory activities were also investigated.

2. Materials and methods

2.1 Materials

Polyvinyl pyrrolidone K88-96 (PVP K88-96; $M_w = 1\,300\,000$) and curcumin (CCM) were purchased from Sigma Aldrich (Shanghai, China). Tetraethylorthosilicate (TEOS), cetyltrimethylammonium bromide (CTAB) and 3-aminopropyltriethoxysilane (APTES) were obtained from Sigma-Aldrich (Shanghai) Trading Co., Ltd. (Shanghai, China). All other chemicals were of analytical grade and obtained from Sinopharm Chemical Reagents Co., Ltd. (Shanghai, China).

2.2 Preparation of CCM-MSNs@PVP nanofiber mats

MSNs were synthesized using the surfactant templating method and the template (CTAB) was finally removed from MSNs by acidic extraction method.[16] Briefly, CTAB (1 g) was dissolved in double-distilled water (480 mL) containing NaOH (0.28 g) at 80 °C. Then TEOS was added dropwise to the mixed solution under vigorous stirring and the process was continued for 20 h. The as-synthesized samples were collected by centrifugation, washed with ethanol and double-distilled water for three times. The samples were refluxed three times in the solution containing ethanol (300 mL) and hydrochloric acid (4 mL) at 78 °C for 24 h to remove CTAB, then centrifuged and washed with ethanol. MSNs were obtained by drying in the drying oven at 80 °C. In order to combine CCM with MSNs, the MSNs were functionalized with amino groups by treating with APTES. MSNs (1 g) was added into anhydrous ethanol (200 mL) and the solution was stirred for 5 min. Then APTES (0.5 mL) was added and the solution was stirred for 8 h at 80 °C. The MSNs-NH_2 was collected by centrifugation, washed with double-distilled water for several times. The drug loading was conducted according to our previous reported protocol,[13] in which the weight ratio of MSNs/curcumin was fixed to be 10/1. In detail, CCM (2 mg) and MSNs-NH_2 (20 mg) were dissolved in ethanol solution (10 mL), followed by stirred at room temperature for 24 h. Then the solution was centrifuged at 10 000 rpm for 8 min. Finally, CCM-loaded MSNs-NH_2 (denoted as CCM-MSNs) powder was repeatedly washed with ethanol and obtained by drying in the drying oven at 80 °C for 8 h.

The electrospun mats with different CCM-MSNs loaded ratios (2, 4 and 8 wt%) were prepared. In a typical process (2 wt% CCM-MSNs loaded PVP nanofiber mats as example), CCM-MSNs (10 mg) was suspended and sonicated in ethanol (5 mL) for 1 min, then PVP (0.5 g) was added into the dispersion with vigorously stirring until the homogeneous suspension formed. The nanofiber mats with different CCM-MSNs contents were similarly prepared by a fixed concentration of PVP (10 w/v). In addition, the pure PVP solution and the PVP solution with MSNs were prepared as well. All the resulting mixtures were degassed to remove the small air bubble and enhance spinnability of the solutions.

For electrospinning, the composite solution was loaded into a syringe with an 18 gauge nozzle and an aluminium foil wrapped copper plate was used as collector, with a distance of 10 cm from the needle tip. The feed rate of syringe pump was controlled at 1.2 mL h^{-1} and the voltage was adjusted to 12 kV. The experiments were performed at room temperature and the relative humidity was approximately 50%. The collected electrospun mats were dried at least 48 h under vacuum to remove the residual solvent prior to further characterization.

2.3 Characterization of the hybrid nanofiber mats

The morphology of the hybrid nanofibers was observed by scanning electron microscope (SEM) with an acceleration voltage of 15 kV at high vacuum. Specimens were fixed on sample stage using a double stick carbon tape. Prior to SEM examination, a thin layer of Au were sputter-coated on the samples in order to prevent abnormal charging. Verification of the CCM-MSNs distribution in the PVP nanofibers was conducted by a JEOL transmission electron microscope (TEM) operated at 200 kV. For TEM specimen preparation, the fiber was collected by putting a small copper grid under the electrospinning nozzle for 10 s during the electrospinning process.

Fourier transform infrared spectroscopy (FTIR) and thermogravimetric analysis (TGA) were employed to characterize physicochemical properties of the hybrid nanofibers. The surface of CCM-MSNs incorporated PVP nanofibers was analyzed by FTIR covering a 4000–700 cm^{-1} infrared range with a resolution of 2 cm^{-1}. TGA measurements were performed to evaluate the thermal behavior of the hybrid nanofibers under

the nitrogen gas protection in the temperature range between 50 and 900 °C at a heating rate of 5 °C min^{-1}.

2.4 *In vitro* cytotoxicity assays

The cytotoxicity of the CCM-MSNs incorporated nanofibers against murine L929 fibrosarcoma cells (L929) was evaluated by Cell Counting Kit-8 (CCK-8) assay. The cells were cultured in Dulbecco's Modified Eagle's Medium (DMEM) supplemented with 10% heat-inactivated fetal bovine serum (FBS) and 100 U mL^{-1} penicillin–streptomycin. The culture condition was maintained at 37 °C in a humidified atmosphere containing 5% CO_2, and the medium was replaced twice a week. Before CCK-8 assay, the nanofiber mats were sterilized under ultraviolet light and then dissolved in the medium to get sample stock solution with concentrations of 5, 10, 20, 40, 80 and 160 μg mL^{-1}. L929 cells were detached by adding 0.25% trypsin (2 mL) containing 0.1% EDTA. The cell suspension was then counted and seeded on 96-well plate at a density of 3000 cells per well. The *in vitro* cytotoxicity assay was carried out at day 1 and 3 after materials adding. For CCK-8 test, the medium was changed and 10% CCK-8 solution (100 μL) was added to each well, and the cells were then incubated for another 1 h. The absorbance was measured at 450 nm using a microplate reader (Biorad, USA). The relative cell viability was defined as the mean percentage of viable cells compared to the control cells.

2.5 *In vitro* antibiotic activity

The bioactivity of hybrid nanofiber mats was determined using an agar disk diffusion bioassay with a MRSA strain (ATCC 29213). Briefly, nanofiber mats (100 mg) with different concentrations of CCM-MSNs (0, 2, 4 and 8 wt%) were respectively dissolved into sterilized PBS (1 mL) to form different CCM-MSNs solutions. Four small circular filter paper pieces were place on the MRSA-seeded agar. Then test samples (50 μL) were dropped on the filter paper pieces. After that, these nutrient agar plates were incubated overnight at 37 °C. All samples were tested in triplicate.

2.6 *In vitro* cell migration

MSNs would reserve within the wound tissue after the hemorrhage process. So we performed this experiment aimed to demonstrate that the residual MSNs would not inhibit the migration of the cells. A sterile steel plate (2 × 1 × 1 mm) was placed onto the middle bottom of a fresh well in a 24-well plate. The L929 cells were seeded on the plate at a density of 50 000 cells per well. Then the culture was maintained at 37 °C in a humidified atmosphere containing 5% CO_2, and the steel plate was replaced 24 h later. A blank area without cells was observed clearly under the microscopy. The number of cells that migrated into the blank areas was then photographed to measure the influence of nanofiber mats on migratory abilities of L929 cells. All experiments were performed in triplicate.

2.7 Hemostasis and whole blood absorption efficiency *in vitro*

The *in vitro* hemostasis ability of the hybrid nanofiber mats was evaluated and compared with that of hemostatic gauze. The equal weight of hybrid nanofiber mats and hemostatic gauze were put into two tubes containing fresh rat blood (1 mL, containing 3.8% sodium citrate) respectively. The weights of these samples were determined when the blood clot formed.

The *in vitro* blood absorption rate was measured according to previous report.[17] Briefly, the materials were dried under vacuum overnight at 80 °C. Then the samples were cut into square size (0.5 cm × 0.5 cm) and weighted as M_1. Afterwards, the fresh rat blood (containing 3.8% sodium citrate) was dropped on the samples until the white nanofiber mats changed to red. The nanofiber mats could rapidly transform to hydrogels when they encounter the blood. The as-formed hydrogel was carefully collected and weighed as M_2. The absorption rate was calculated by the following formula:

$$\text{Absorption rate} = \frac{M_2 - M_1}{M_1} \times 100\%$$

After weighting, the blood–hydrogel composites were observed by a light microscope (Leica Microsystems, Germany).

2.8 Evaluation of the effect on the plasmatic phase of coagulation

The coagulant activity of the hybrid nanofibers was investigated through two typical coagulation tests named activated partial thromboplastin time (APTT) and prothrombin time (PT). The experiment was carried out using a reagent kit made by Nanjing jiancheng with a semi-automatic coagulation analyzer. The whole blood was collected from the jugular vein of Wistar rats by the 5% isoflurane anesthesia and then immediately mixed with a one-tenth volume of 3.8% (w/v) sodium citrate. With the centrifugation at 2000 g for 10 min at 4 °C, the platelet poor plasma (PPP) was collected for coagulation tests. During the APTT test, the plasma (50 μL) mixed with APTT reagent (50 μL) were incubated for 3 min at 37 °C. After addition of pre-warmed (37 °C) calcium chloride (100 μL), the CCM-MSNs incorporated nanofiber mats were immediately immersed in the plasma. The time from this addition to clot formation was defined as the APTT. For the PTT test, citrated plasma (100 μL) and the hybrid mats were added to the PT reagent (Dade® Innovin®) (200 μL, incubated for 1 min at 37 °C). The time from the plasma-reagent mixing to clot formation was recorded as the PT. The test without any materials addition was also performed and used as negative control simultaneously.

2.9 Liver injury experiment

The study protocols were approved by Institutional Animal Care and Use Committee (IACUC) of Fudan University and all the animals were treated in accordance with the Fudan University Pudong Medical Center's guidelines. Male ICR mice weighing 25–30 g were purchased from Shanghai Slac laboratory animal co., LTD, China. The nanofiber mats possessed both good

morphology and low cytotoxicity was used for animal tests. For all model surgery, the mice were anesthetized and maintained by 3–5% isoflurane with a face mask. At the end of the experiment, all animals were euthanized with an overdose intravenous injection of pentobarbital.

The anesthetized ICR mice were shaved and placed on their backs. The abdomen cavity was then opened to expose the liver. A penetrating incision of 0.5 cm in length was made with a surgical scalpel on the left medial lobe of liver. After 3 s bleeding, CCM-MSNs@PVP nanofiber mats (0.5 × 0.5 cm) were administrated on the injury site. The clotting time was precisely recoded at the beginning of the bleeding. When the hemostasis process completed, the incision site was washed with saline solution (5 mL) to remove residual materials.

To evaluate the healing effect of nanofiber mats on liver injury, three injured liver from different mice were dissected after the hemostasis process completed and then immersed in the 4% phosphate buffered formalin and processed as histological samples. Another three mice underwent the surgery were continued to feed for two weeks. Then these injured livers from different mice was dissected and handled as the previous processing. After that 3 μm thick sections with H&E (hematoxylin and eosin) and Masson's Trichrome Stain were observed by a light microscope (Leica Microsystems, Germany).

2.10 Statistical analysis

All the data were represented as the means ± standard deviation (SD). Statistical difference was analyzed using one-way analysis of variance (ANOVA). A value of $*p < 0.05$ was considered to be statistically significant.

3. Results and discussions

3.1 Characterization of CCM-MSNs@PVP hybrid nanofiber mats

The schematic fabrication process of CCM-MSNs@PVP hybrid nanofiber mats is shown in Fig. 1. As previously report[18] demonstrated, the direct loading curcumin into MSNs could not yield high loading content, thus the MSNs were functionalized with amino before the loading process, which can be facilitate by the intermolecular force between polar groups of curcumin and amine groups.[19] CCM-MSNs@PVP hybrid nanofiber mats were prepared by blended electrospinning of CCM-MSNs and PVP solution. Fig. 2 shows the SEM and TEM images of the fabricated nanofibers with different ratios of CCM-MSNs (0, 2, 4 and 8 wt%) and MSNs@PVP (4 wt% MSNs). From these SEM images, it can be seen that the surface of the hybrid nanofibers containing 4 wt% MSNs and CCM-MSNs (Fig. 2C and D) was a bit rough without beads defects, which is similar to that observed in pure PVP and 2 wt% CCM-MSNs nanofibers (Fig. 2A and B). However, after incorporated with more CCM-MSNs, the hybrid nanofibers containing 8 wt% CCM-MSNs showed some beads defects (Fig. 2E). TEM images confirmed that the incorporated CCM-MSNs were well distributed within the hybrid nanofibers with lower CCM-MSNs contents (Fig. 2F and G). However, the aggregation of nanoparticles could be observed in the hybrid nanofibers with high CCM-MSNs contents (Fig. 2J). Thus, we deduced that the 4% loading content of CCM-MSNs in composite nanofibers might be the optimal ratio in this study.

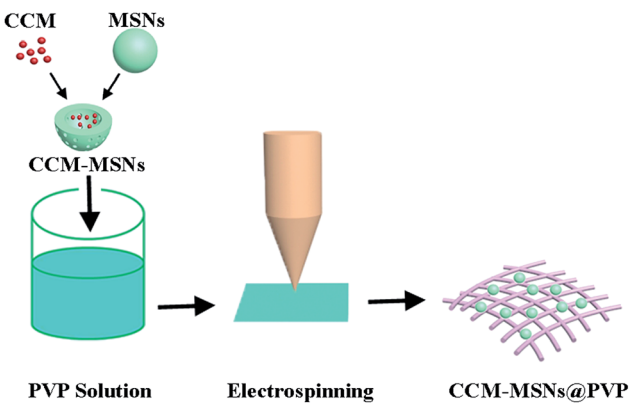

Fig. 1 Schematic illustration of the formation of curcumin-loaded mesoporous silica incorporated nanofiber mats.

The FTIR spectra presented in Fig. 3A show the characteristic absorption peaks of different components in the hybrid nanofibers. For the pure PVP, the broad peak around 3435 cm^{-1} was assigned to –O–H stretching vibration, while the peaks observed at 2949, 1661 and 1288 cm^{-1} were attributed to –C–H, –C═O, –C–N– stretching vibration, respectively. The spectrum of MSNs showed important characteristic absorption band at 800, 960 (Si–O–Si symmetric stretching vibration) and 1100 cm^{-1} (Si–O–Si asymmetric stretching vibration). Additionally, the vibration of Si–OH was also found around 3432 cm^{-1}. The CCM-MSNs@PVP nanofibers exhibited similar FTIR spectra with pure PVP and MSNs and also share their characteristic peaks at 1095, 1290 and 1659 cm^{-1}, suggesting the successful incorporating of CCM-MSNs into PVP nanofibers.

Results of thermogravimetric analyses of pure PVP and CCM-MSNs@PVP nanofibers were shown in Fig. 3B. It was observed that curves of all samples had a slight weight loss of about 10% to 15% under 100 °C, which is due to the removal of residual moisture. Additionally, PVP and CCM-MSNs@PVP nanofiber samples showed a distinct weight loss in the range of 400–450 °C due to the degradation of the polymer molecules. At 900 °C, the weight residue for 4 wt% CCM-MSNs@PVP nanofibers was about 4%, and the pure PVP nanofibers showed no residue at 900 °C. This difference is due to high thermal stability of MSNs, which clearly indicated the successful incorporation of MSNs at around 4 wt%. The onset temperature of the pure PVP was calculated to be 394 °C, while the nanofibers incorporated with MSNs displayed onset temperature at 405 °C. This result is consistent with a previous study.[20] The higher onset temperature of the CCM-MSNs@PVP nanofibers was partly attributed to the formation of some weak bonding between PVP and MSNs. The weight residue for 8 wt% CCM-MSNs@PVP nanofibers was about 7% when the temperature reached 900 °C, while the weight residue for 2 wt% CCM-MSNs@PVP nanofibers was about 1% at the same temperature.

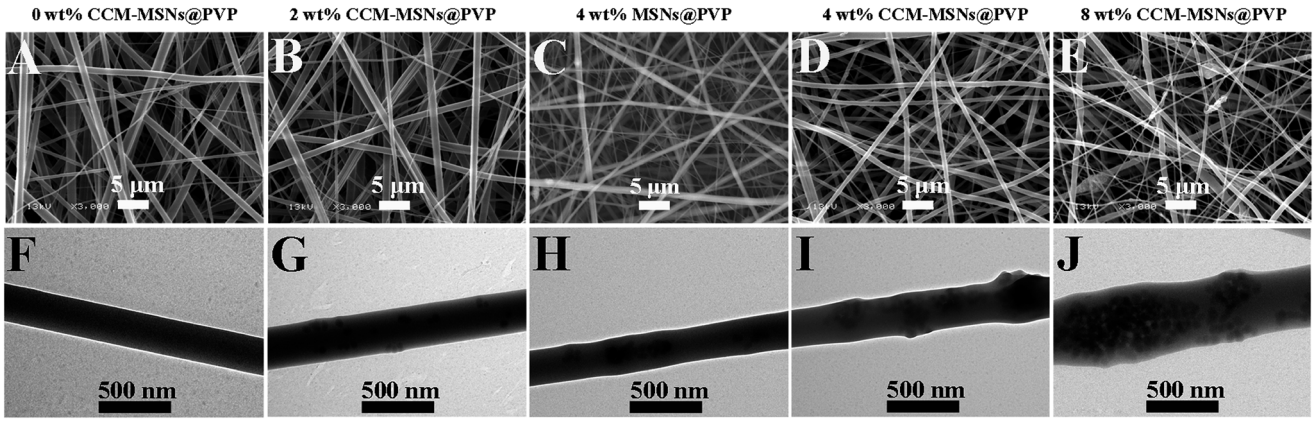

Fig. 2 SEM images of PVP nanofibers with various CCM-MSNs ratios of (A) 0 wt%, (B) 2 wt%, (D) 4 wt% and (E) 8 wt% and MSNs ratio of (C) 4 wt%. TEM images of PVP nanofibers with various CCM-MSNs ratios of (F) 0 wt%, (G) 2 wt%, (I) 4 wt%, (J) 8 wt% and MSNs ratio of (H) 4 wt%.

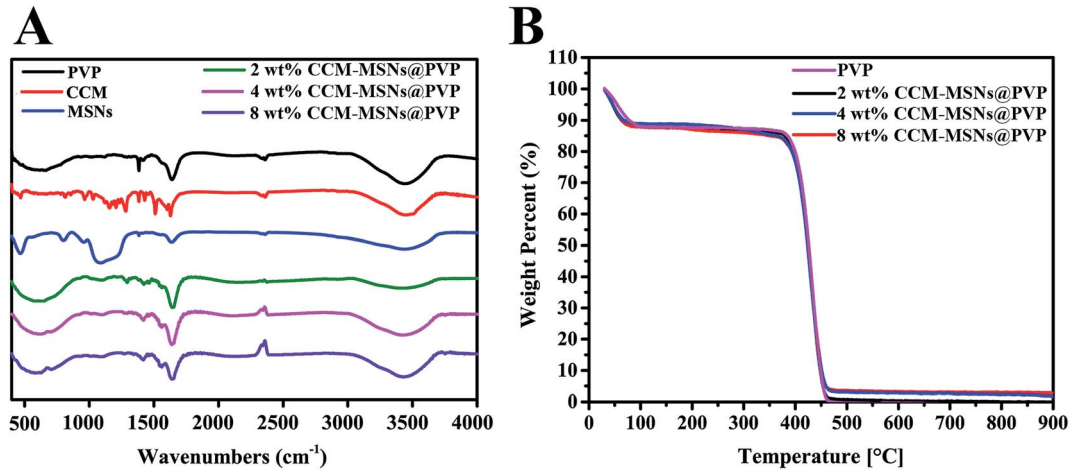

Fig. 3 (A) The FTIR spectra for the MSNs, pure PVP and CCM-MSNs@PVP nanofibers. (B) Results of thermogravimetric analyses of pure PVP, MSNs and CCM-MSNs@PVP nanofiber mats.

3.2 *In vitro* cytotoxicity assay

The cytotoxicity of materials was performed by evaluating the viability of L929 cells after treatment with different hybrid nanofibers using CCK-8 method. As shown in Fig. 4A and B, all the nanofibers tested showed no obvious toxicity towards L929 cells after incubation for 1 day and 3 days. Even at the concentration of 160 μg mL^{-1}, the cell viabilities for different nanofibers were large than 80%, indicating the good biocompatibility and low cytotoxicity of the fabricated hybrid nanofibers.

3.3 *In vitro* antibacterial activity

In this assay, the diameter of inhibition zones of nanofiber mats was used to evaluate the bacterial activity. Inhibition zones were not observed around the pure PVP (Fig. 4C(a)) and 4 wt% MSNs@PVP nanofibers (Fig. 4C(b)). In contrast, the diameters of inhibition zones were 10.56, 10.83 and 11.43 mm for the nanofibers with 2, 4 and 8 wt% CCM-MSNs respectively (Fig. 4C). After incubation for 48 h, these inhibition zones were also observed clearly which illustrated the persistent antibacterial ability of these doped nanofiber mats (Fig. 4D). In previous studies, curcumin was used for wound care and antimicrobial activity.[21,22] The prepared hybrid nanofiber mats can provide good antimicrobial effect due to the loaded curcumin. In Indian and China, the turmeric plant has been used throughout history as a dietary spice and coloring agent. An oral doses as high as 12 grams per day tolerated safely was illustrated in clinical trials for myriad disease entities.[23] Moreover, several studies indicated that heavy metal ion such as Ag and Cu may cause potential influence on mouse organs.[24,25] Based on the above reasons, CCM-MSNs@PVP nanofibers would be potential candidate hemostatic materials for wound healing applications.

3.4 *In vitro* cell migration

For *in vitro* cell migration test, the 4 wt% CCM-MSNs@PVP nanofibers was selected for animal tests. As seen from Fig. 5, all the tested samples showed no remarkable inhibiting actions compared to control group. Fig. 5A shows the blank area on the

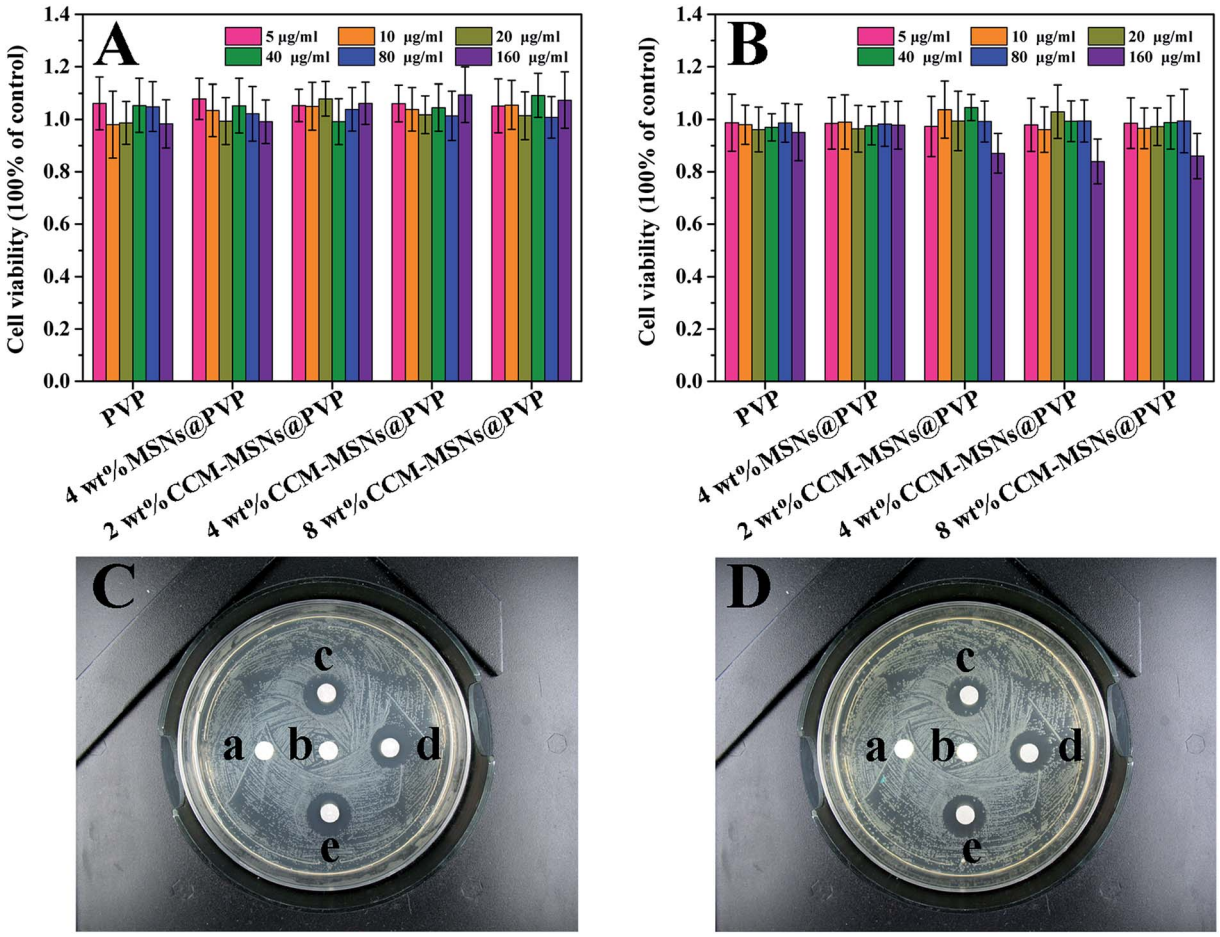

Fig. 4 Cytotoxicity tests from CCK-8 assays of cell viability in DMED with various CCM-MSNs ratios. The proliferation of L929 cells in pure PVP medium and CCM-MSNs@PVP medium for (A) 1 d and (B) 3 d. Bacterial growth inhibition on agar plate after incubation for (C) 12 h and (D) 48 h. (a) Pure PVP; (b) 4 wt% MSNs@PVP nanofiber mats; (c) 2 wt% CCM-MSNs@PVP nanofiber mats; (d) 4 wt% CCM-MSNs@PVP nanofiber mats; (e) 8 wt% CCM-MSNs@PVP.

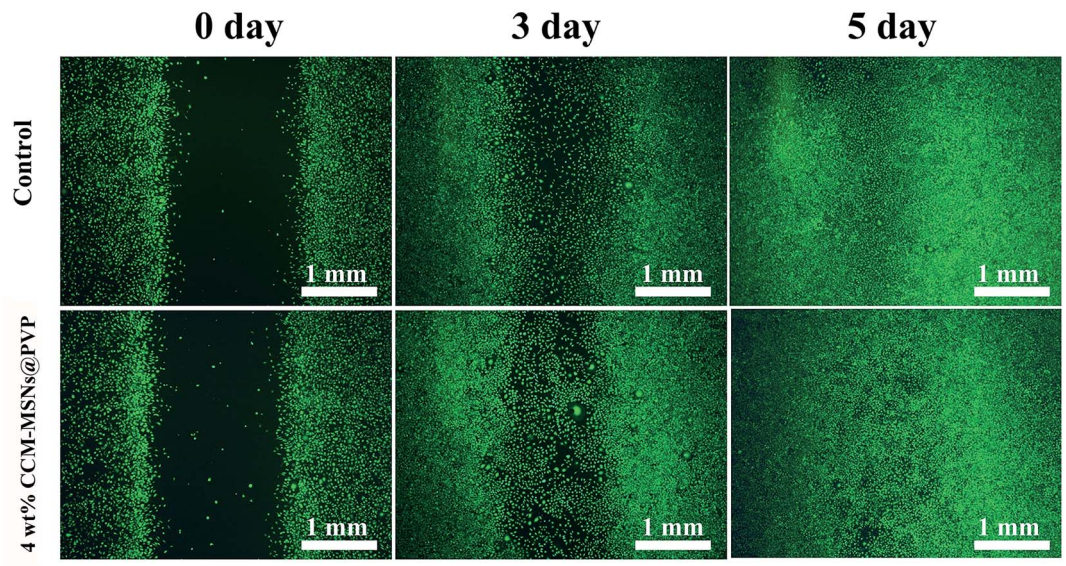

Fig. 5 The proliferation of L929 cells in unconditioned medium and 4 wt% CCM-MSNs@PVP medium for 0, 3 and 5 d.

middle bottom clearly. L929 cells distributed on the both sides of the blank area begun to proliferate on the 3 day, some proliferated cells appeared at the blank area. At day 5, more and more cells proliferated and the blank area became vaguer than that at day 3. This result illustrated that the prepared nanofiber mats would not affect the wound healing in the process of hemostatic functions compared with the blank group.

3.5 Hemostasis and whole blood absorption efficiency *in vitro*

High water adsorption capacity plays a significant role in coagulation process, which facilitates to concentrate the haemocytes and fibrin in hemorrhaging blood at the injury site, resulting in a close interaction of platelets towards the damaged

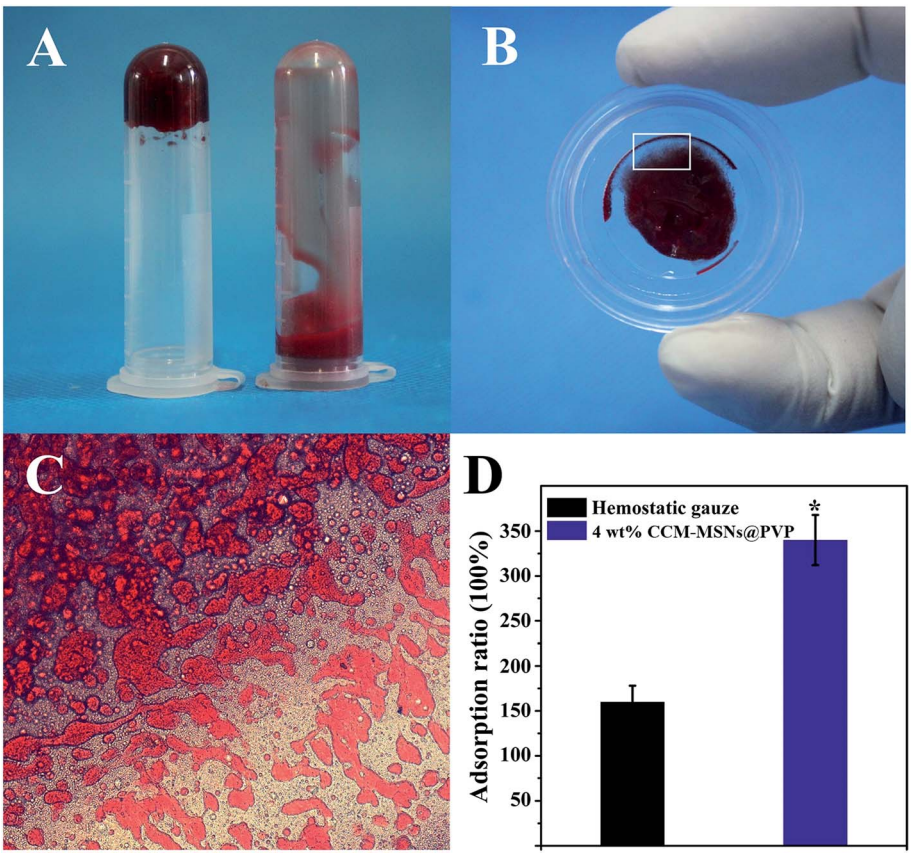

Fig. 6 (A) The formation of blood clot *in vitro* (left, CCM-MSNs@PVP nanofiber mats; right, common hemostatic gauze). (B) The formation of hydrogel composite. (C) The structure of the hydrogel composite under the microscope. (D) The whole blood absorption efficiency of common hemostatic gauze (black) and 4 wt% CCM-MSNs@PVP nanofiber mats (blue). *$p < 0.05$, statistical significance.

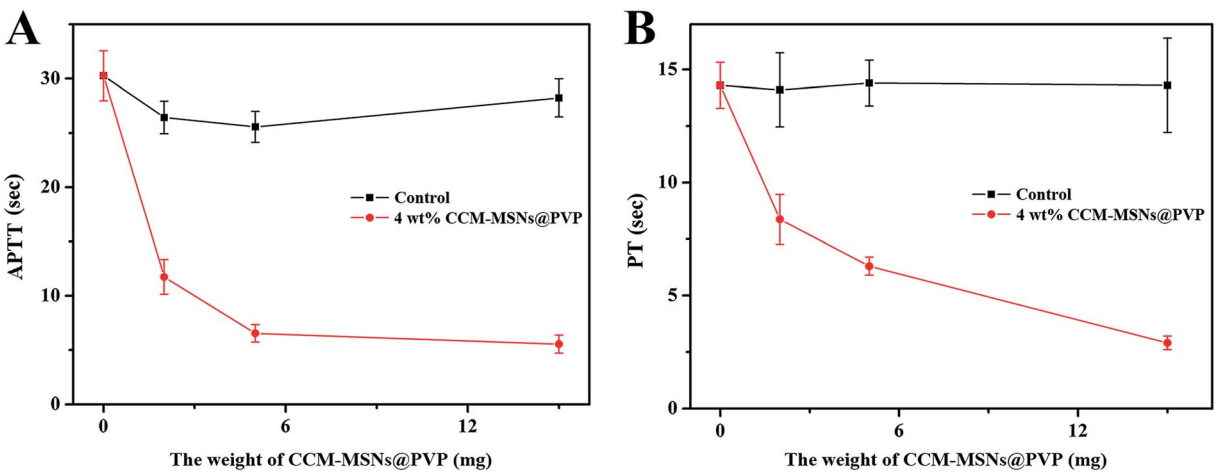

Fig. 7 (A) The time from this addition to clot formation. (B) The time from the plasma-reagent mixing to clot formation.

vessels and further accelerate the clotting process.[26] It is worth noting that a hydrogel composite was observed once the CCM-MSNs@PVP nanofibers meet the test liquid, which can promote the formation of blood clot (Fig. 6A, left). Compared with the CCM-MSNs@PVP nanofiber mats, common hemostatic gauze did not possess the same effect (Fig. 6A, right). The whole blood absorption ratios of hemostatic gauze and CCM-MSNs@PVP nanofiber mats were presented in Fig. 6. Clearly, the CCM-MSNs@PVP nanofibers caused a maximum whole blood absorption ratio about 300% of the weight, whereas the value of hemostatic gauze was only 150% (Fig. 6D). These results showed that the hybrid nanofiber mats could achieve rapid hemostasia by promoting clotting.

3.6 Evaluation of the effect on the plasmatic phase of coagulation

PT and APTT tests are the important clinic assays to determine the extrinsic and intrinsic pathway of coagulation. The time recorded in the test compared to the control was used to determine the clotting tendency of blood. Hence, by adding prepared materials into the tested system, we can get the detailed data about materials activation in blood plasma coagulation and figure out how the materials affect the clotting system *in vivo*. The results of PT and APTT tests were concluded in Fig. 7. It was clearly seen that the coagulation time of MSNs@PVP nanofibers in PT and APTT test were lower than that of control and decreased with the increased in the addition amount of as-prepared materials, suggesting that the hybrid mats had a positive impact on the rapid hemostasis.

3.7 Liver injury experiment

The hemorrhage was mainly occurred in the aorta, vena cava and some vessel-abundant organs (spleen and liver as example). So we performed an animal hemorrhage model to investigate the hemostasis efficacy of the liver. The whole experiment process was recorded by digital camera and presented in the

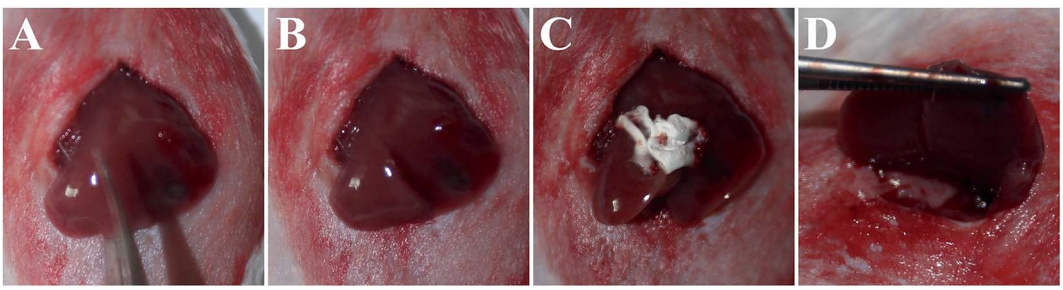

Fig. 8 (A) The exposed left medial lobe of intact liver. (B) Profuse bleeding immediately after injury creation. (C) Treatment with CCM-MSNs@PVP nanofiber mats over the site of injury. (D) Bleeding ceased after CCM-MSNs@PVP nanofiber mats was applied over the wound.

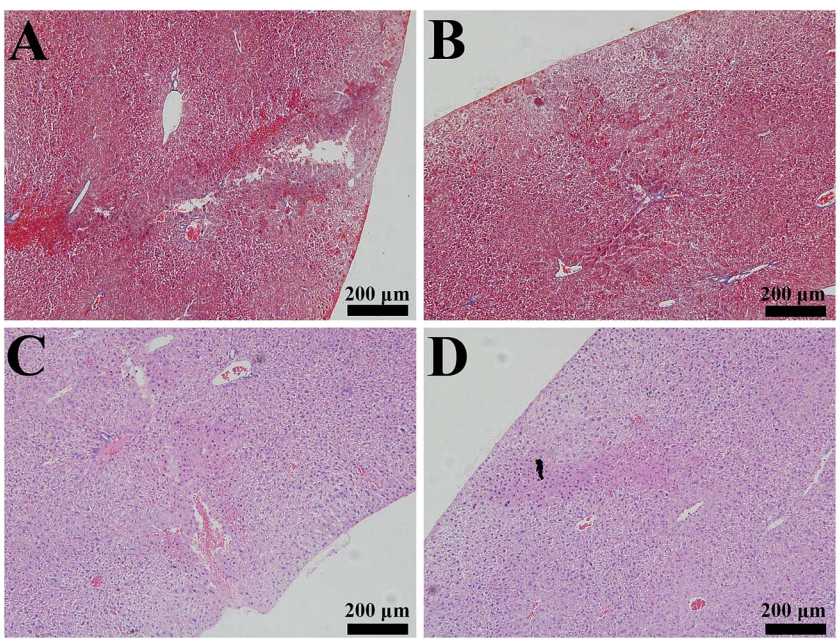

Fig. 9 Histopathology of liver. H&E staining of (A) the injured liver after the hemostasis process completed and (B) the injured liver after two weeks. Masson's trichrome staining of (C) the injured liver after the hemostasis process completed and (D) the injured liver after two weeks.

Fig. 8. A 5 mm longitudinal incision was made by using a pair of sterile scissors (Fig. 8A and B). A rapid hemostasis in animal hemorrhage model was clearly observed by treatment of 4 wt% CCM-MSNs@PVP hybrid nanofibers (Fig. 8C and D). We also found that once the CCM-MSNs@PVP contact with blood, it swelled and transformed to hydrogel composite, forming a hydrophilic membrane on the surface of wound. Interestingly, hemostasis was completed after the hydrogel composite formation. This result implied that the hemostatic mechanism was closely related with the composite formation between blood and materials. The melting nanofiber mats was very sticky. This can help combine the separated liver tissue together tightly. No blood was observed when using surgical tweezers raise the damaged liver tissue from the bottom. These results illustrated that the hemostatic effect of nanofiber mats was very effective. After finishing the hemostasis test *in vivo*, these incisions were stitched conventionally. No mice underwent surgery were found infection before the surgical wound healed. The result indicated that the nanofiber mats also possessed satisfactory antibacterial characteristics.

In order to explore the instinct structure of the hydrogel composite and investigate the mechanism of CCM-MSNs@PVP induced hemostasis, the histological examination was conducted in the hybrid nanofibers and the injured liver. Fig. 9A and C showed the structure of the injury liver dissected after the hemostasis process completed. A great number of haemocytes were observed and the distribution of these cells is uniform in the composite, implying a fact that the blood was firstly absorbed into CCM-MSNs@PVP nanofibers to form a hydrosol composite and then activated to the hydrogel for hemostasis complement. The lesion of injured liver also showed significant cell accumulation in the incision, which indicated the preformed hydrosol could diffuse into the wound with tunable shapes and promote the hemostasis inside the tissue. Fig. 9B and D illustrated the H&E staining and Masson's trichrome staining of the injury liver dissected after two weeks. No significant morphological changes such as severe and extensive hepatocellular damage were observed in the damaged livers. Only a few numbers of haemocytes were observed around the wound. The healing of the damaged liver which was dealt with the prepared nanofiber mats illustrated the good biocompatibility of the materials.

4. Conclusion

In summary, the curcumin-loaded mesoporous silica incorporated nanofiber mats were fabricated by electrospinning, and their potential for hemorrhage control and antibacterial treatment were systemically evaluated through *in vitro* and *in vivo* studies. The loading of CCM-MSNs in CCM-MSNs@PVP not only affect the morphology of the fabricated nanofibers, but also exert influence on the biological functions. The hybrid nanofibers with higher CCM-MSNs contents showed enhanced antimicrobial efficacy. The whole blood absorption test demonstrated that the hybrid nanofibers possessed relatively high liquid absorption rates. The PT and APTT results revealed that the hybrid nanofibers can activate both intrinsic and extrinsic coagulation pathways. Moreover, the *in vivo* studies further confirmed that the hybrid nanofibers can induce the significant haemocytes aggregation in the coagulated composite and produce the desirable hemorrhage control in liver injury. The rapid hemostasis induced by hybrid nanofibers is probably due to their extremely high water absorption ability. The histological results revealed that the blood was firstly absorbed into the hybrid nanofibers to form hydrosol composite and then activated by clotting system to complete the hemostasis. In addition, the fabricated hybrid nanofibers also showed good antibacterial effect both *in vitro* and *in vivo*. Thus, the developed hybrid nanofibers would be potential candidate hemostatic materials for wound healing applications.

Acknowledgements

This study was funded by the Disciplines Group Construction Project of Pudong Health Bureau of Shanghai (PWZxq2014-03). The authors are grateful for the financial support from the National Natural Science Foundation of China (31271028, 31570984), International Cooperation Fund of the Science and Technology Commission of Shanghai Municipality (15540723400).

References

1 V. A. Kumar, N. L. Taylor, A. A. Jalan, L. K. Hwang, B. K. Wang and J. D. Hartgerink, *Biomacromolecules*, 2014, **15**, 1484–1490.
2 H. B. Alam, D. Burris, J. A. DaCorta and P. Rhee, *Mil. Med.*, 2005, **170**, 63–69.
3 M. C. Neuffer, J. McDivitt, D. Rose, K. King, C. C. Cloonan and J. S. Vayer, *Mil. Med.*, 2004, **169**, 716–720.
4 C. L. Dai, Y. Yuan, C. S. Liu, J. Wei, H. Hong, X. S. Li and X. H. Pan, *Biomaterials*, 2009, **30**, 5364–5375.
5 C. L. He, W. Nie and W. Feng, *J. Mater. Chem. B*, 2014, **2**, 7828–7848.
6 K. Jiang, Y. Z. Long, Z. J. Chen, S. L. Liu, Y. Y. Huang, X. Y. Jiang and Z. Q. Huang, *Nanoscale*, 2014, **6**, 7792–7798.
7 H. Wang, M. Li, J. Hu, C. Wang, S. Xu and C. C. Han, *Biomacromolecules*, 2013, **14**, 954–961.
8 B. K. Gu, S. J. Park, M. S. Kim, Y. J. Lee, J. Kim and C. Kim, *Int. J. Biol. Macromol.*, 2016, **82**, 89–96.
9 K. Madhumathi, P. T. S. Kumar, S. Abhilash, V. Sreeja, H. Tamura, K. Manzoor, S. V. Nair and R. Jayakumar, *J. Mater. Sci.: Mater. Med.*, 2010, **21**, 807–813.
10 S. Liu, Y. C. Kau, C. Y. Chou, J. K. Chen, R. C. Wu and W. L. Yeh, *J. Membr. Sci.*, 2010, **355**, 53–59.
11 A. Lamikanra, J. L. Crowe, R. S. Lijek, B. W. Odetoyin, J. Wain, A. O. Aboderin and I. N. Okeke, *BMC Infect. Dis.*, 2011, **11**, 312.
12 D. G. Yu, X. X. Sheng, B. W. C, K. White, L. M. Zhu and S. W. A. Bligh, *Nanotechnology*, 2009, **20**, 55104–55109.
13 W. Feng, W. Nie, C. L. He, X. J. Zhou, L. Chen, K. X. Qiu, W. Z. Wang and Z. Q. Yin, *ACS Appl. Mater. Interfaces*, 2014, **6**, 8447–8460.

14 W. Feng, X. J. Zhou, C. L. He, K. X. Qiu, W. Nie, L. Chen, H. S. Wang, X. M. Mo and Y. Z. Zhang, *J. Mater. Chem. B*, 2013, **1**, 5886–5898.
15 K. X. Qiu, B. Chen, W. Nie, X. J. Zhou, W. Feng, W. Z. Wang, L. Chen, X. M. Mo, Y. Z. Wei and C. L. He, *ACS Appl. Mater. Interfaces*, 2016, **8**, 4137–4148.
16 X. J. Zhou, W. Feng, K. X. Qiu, L. Chen, W. Z. Wang, W. Nie, X. M. Mo and C. L. He, *ACS Appl. Mater. Interfaces*, 2015, **7**, 15777–15789.
17 C. L. Dai, C. S. Liu, J. Wei, H. Hong and Q. H. Zhao, *Biomaterials*, 2010, **31**, 7620–7630.
18 R. Kotcherlakota, A. K. Barui, S. Prashar, M. Fajardo, D. Briones, A. Rodriguez-Dieguez, C. R. Patra and S. Gomez-Ruiz, *Biomater. Sci.*, 2016, **4**, 448–459.
19 V. S. Bollu, A. K. Barui, S. K. Mondal, S. Prashar, M. Fajardo, D. Briones, A. Rodríguez-Diéguez, C. R. Patra and S. Gómez-Ruiz, Curcumin-loaded silica-based mesoporous materials: synthesis, characterization and cytotoxic properties against cancer cells, *Mater. Sci. Eng., C*, 2016, **63**, 393–410.
20 N. Sahiner, N. Pekel and O. Guven, *React. Funct. Polym.*, 1999, **39**, 139–146.
21 A. E. Krausz, B. L. Adler, V. Cabral, M. Navati, J. Doerner, R. A. Charafeddine, D. Chandra, H. Liang, L. Gunther, A. Clendaniel, S. Harper, J. M. Friedman, J. D. Nosanchuk and A. J. Friedman, *Nanomed. Nanotech. Biol. Med.*, 2015, **11**, 195–206.
22 D. Akbik, M. Ghadiri, W. Chrzanowski and R. Rohanizadeh, *Life Sci.*, 2014, **116**, 1–7.
23 S. C. Gupta, S. Patchva and B. B. Aggarwal, *AAPS J.*, 2013, **15**, 195–218.
24 D. D. Sun, W. W. Zhang, N. Li, Z. W. Zhao, Z. P. Mou, E. Yang and W. Y. Wang, *Mater. Sci. Eng., C*, 2016, **63**, 522–534.
25 S. Mallick, S. Sharma, M. Banerjee, S. S. Ghosh, A. Chattopadhyay and A. Paul, *ACS Appl. Mater. Interfaces*, 2012, **4**, 1313–1323.
26 S. Y. Ong, J. Wu, S. M. Moochhala, M. H. Tan and J. Lu, *Biomaterials*, 2008, **29**, 4323–4332.